


Uncertainty quantification and sensitivity analysis of an arterial wall mechanics model for evaluation of vascular drug therapies

Maarten H. G. Heusinkveld¹  · Sjeng Quicken¹ · Robert J. Holtackers³ ·
Wouter Huberts¹ · Koen D. Reesink¹ · Tammo Delhaas¹ · Bart Spronck^{1,2}

Received: 18 June 2017 / Accepted: 17 July 2017 / Published online: 28 July 2017
© The Author(s) 2017. This article is an open access publication

Abstract Quantification of the uncertainty in constitutive model predictions describing arterial wall mechanics is vital towards non-invasive assessment of vascular drug therapies. Therefore, we perform uncertainty quantification to determine uncertainty in mechanical characteristics describing the vessel wall response upon loading. Furthermore, a global variance-based sensitivity analysis is performed to pinpoint measurements that are most rewarding to be measured more precisely. We used previously published carotid diameter–pressure and intima–media thickness (IMT) data (measured in triplicate), and Holzapfel–Gasser–Ogden models. A virtual data set containing 5000 diastolic and systolic diameter–pressure points, and IMT values was generated by adding measurement error to the average of the measured data. The model was fitted to single-exponential curves calculated from the data, obtaining distributions of constitutive parameters and constituent load bearing parameters. Additionally, we (1) simulated vascular drug treatment to assess the relevance of model uncertainty and (2) evalu-

ated how increasing the number of measurement repetitions influences model uncertainty. We found substantial uncertainty in constitutive parameters. Simulating vascular drug treatment predicted a 6% point reduction in collagen load bearing (L_{coll}), approximately 50% of its uncertainty. Sensitivity analysis indicated that the uncertainty in L_{coll} was primarily caused by noise in distension and IMT measurements. Spread in L_{coll} could be decreased by 50% when increasing the number of measurement repetitions from 3 to 10. Model uncertainty, notably that in L_{coll} , could conceal effects of vascular drug therapy. However, this uncertainty could be reduced by increasing the number of measurement repetitions of distension and wall thickness measurements used for model parameterisation.

Keywords Arterial wall mechanics · Constitutive modelling · Uncertainty quantification · Sensitivity analysis · Vascular ultrasound

✉ Maarten H. G. Heusinkveld
m.heusinkveld@maastrichtuniversity.nl
Tammo Delhaas
tammo.delhaas@maastrichtuniversity.nl
Bart Spronck
b.spronck@maastrichtuniversity.nl

¹ Department of Biomedical Engineering, CARIM School for Cardiovascular Diseases, Maastricht University, Universiteitssingel 50, Room 3.358, 6229 ER Maastricht, The Netherlands
² Department of Biomedical Sciences, Faculty of Medicine and Health Sciences, Macquarie University, Sydney, NSW, Australia
³ Department of Radiology, CARIM School for Cardiovascular Diseases, Maastricht University, Maastricht, The Netherlands

1 Introduction

Arterial stiffening is a major determinant of hypertension and vice versa (Humphrey et al. 2016). Treatment options for arterial stiffening can roughly be divided into two categories: (1) prescribing drugs that lower blood pressure and consequently reverse the arterial structural remodelling that occurs with hypertension, or (2) prescribing drugs that directly affect the arterial wall structure (Townsend et al. 2015). The second category includes cross-link breaking drugs that target the arterial collagen network (Kass et al. 2001; Wolffenbuttel et al. 1998). These types of drugs aim to break down the advanced glycation end products (AGE) that form cross-links between collagen molecules (McNulty et al. 2007; Kass et al. 2001; Brownlee 1995). The desired mechanical effect

of such drug therapies is to reverse pressure load bearing from a stiff, collagen-dominated phenotype to a less stiff, elastin-dominated phenotype, resulting in a decrease in material stiffness (O'Rourke and Hashimoto 2007; Wolffenbuttel et al. 1998).

In vivo assessment of the performance of vascular drugs has proved to be cumbersome (Engelen et al. 2013). Arterial stiffness is typically quantified by measuring carotid–femoral pulse wave velocity, or by local assessment of arterial distensibility (Kass et al. 2001; Wolffenbuttel et al. 1998). A limitation of these indices is their blood pressure dependence, for which an incremental change in these indices could occur solely from a change in blood pressure (Spronck et al. 2015b). In addition, arterial stiffness measurements as such do not yield insight into the effect of a drug at microstructural level, nor do they resolve whether the load bearing phenotype is collagen- or elastin-dominated.

A potential solution to this problem lies in the use of computer models that simulate stress–strain behaviour of arteries using physical constitutive relations (Holzapfel et al. 2000). In such models, it might be possible to analyse the individual contribution of both elastin and collagen to the overall mechanical response of the vessel wall. *Ex vivo* studies on human carotid arteries, performed in the laboratory, reported good agreement between constitutive model computations and biaxial tensile tests (Sommer and Holzapfel 2012; Sommer et al. 2010). If such models could be parameterised using non-invasive measurements in patients, they could be used to evaluate the mechanics of the vessel wall patient-specifically. Several studies have attempted to use *in vivo* data to parameterise constitutive models of the arterial wall, as reviewed in Spronck et al. (2015a). Typically, diameter, pressure, and intima–media thickness measurements at the carotid artery are used to fit such models (Spronck et al. 2015a). Generally, noise in those measurements will hamper patient-specific evaluation of arterial wall mechanics.

In this study, we aim to (1) assess how measurement uncertainty propagates into uncertainty of mechanical characteristics, estimated using a model of arterial wall mechanics and (2) pinpoint the measurements responsible for the largest spread in mechanical characteristics through sensitivity.

Uncertainty quantification and sensitivity analysis are considered indispensable tools to ensure credibility of computer model-based predictions (National Research Council 2012). We explicitly focus on two types of mechanical characteristics: (1) constitutive parameters, describing the mechanical properties of collagen and elastin, and (2) constituent load bearing parameters, describing to which extent the blood pressure load is borne per constituent. The latter parameters are considered outcome parameters, obtained by evaluating the model using the best-fit set of constitutive parameters (Fig. 1, left pane). For these purposes, a large set of virtual pressure (P), diameter (D), and intima–

media thickness (IMT) measurements will be generated by sampling the measurement distributions of previously published P , D , and IMT measurements in healthy volunteers (Holtackers et al. 2016). For each D – P sample, we will obtain continuous D – P curves over the diastolic–systolic pressure range, using the single-exponential function introduced by Hayashi et al. (1980). Holzapfel–Gasser–Ogden constitutive models will be fitted to these data (Holzapfel et al. 2000), and uncertainty quantification will be used to quantify the spread in the estimated mechanical characteristics, given the measurement noise (Fig. 1, left pane). A sensitivity analysis will be performed to determine how noise in the *individual* measured variables propagates into uncertainty in the model-predicted mechanical characteristics. The relevance of the model output uncertainty magnitude, which results from uncertainty in the model parameters, will be assessed by simulating the effect of AGE-breaker treatment on changes in collagen load bearing behaviour in our model (Fig. 1, right pane).

2 Methods

2.1 Constitutive model definition

To identify mechanical characteristics of the carotid artery wall, we used the Holzapfel–Gasser–Ogden constitutive model describing passive carotid artery wall mechanics (Holzapfel et al. 2000). This model was chosen on the one hand for its low number of parameters and on the other hand for its feasibility in identifying mechanical characteristics when fitted to clinically obtained distensibility data (Spronck et al. 2015a). Here, we will give a brief description of the model. For more details, we refer to Appendix A1.

In the model, the carotid artery is considered to be a thick-walled incompressible tubular structure composed of a mixture of two components: (1) elastin, assumed mechanically isotropic, and (2) collagen fibres, assumed mechanically orthotropic. Collagen was modelled by two families of fibres that are helically oriented at an angle of $+\beta_0$ and $-\beta_0$ with respect to the circumferential direction (Fig. 2). Elastin and collagen were assumed to operate in parallel. Furthermore, we assumed that there is only deformation along the principal axes, i.e. no shear. Mechanical properties of the arterial wall components are expressed in terms of strain energy functions.

The strain energy function (SEF) used for elastin (W_{elast}) is given by

$$W_{\text{elast}} = c_{\text{elast}}(I_1 - 3), \quad (1)$$

with I_1 the first invariant of the Green–Lagrange strain tensor, given by $I_1 = \lambda_{rr}^2 + \lambda_{\theta\theta}^2 + \lambda_{zz}^2$, with λ the stretch in the radial (r) direction, circumferential (θ) direction, and axial

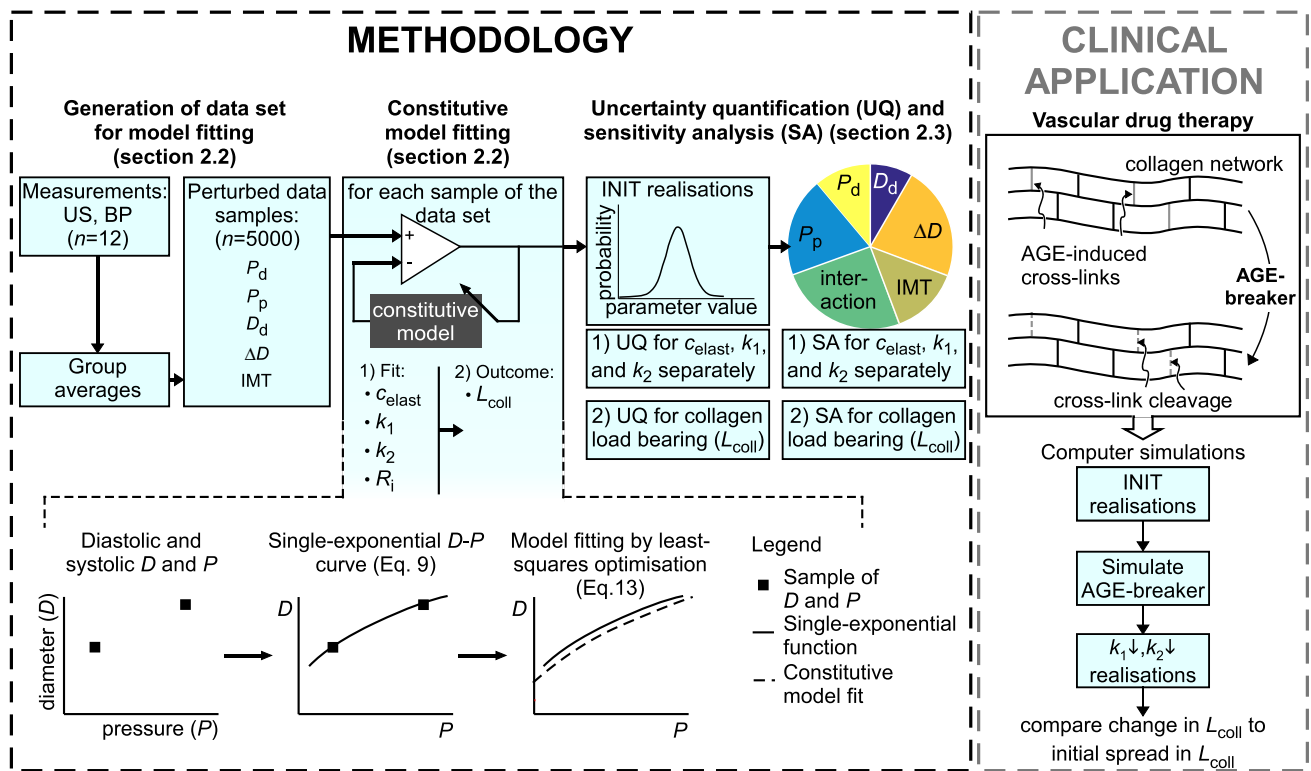


Fig. 1 Outline of the current study, involving (1) uncertainty quantification (UQ) and sensitivity analysis (SA) of a constitutive model of arterial wall mechanics (methodology, *left*) and (2) assessment of the relevance of the model output uncertainty when evaluating the effects of vascular drug treatment (clinical application, *right*). *Left* group-averaged measured variables were obtained from a previous study, measuring twelve healthy subjects. The effect of measurement uncertainty on measured variables was included by perturbing group-averaged variables based on their measurement uncertainty. Within the margins of measurement uncertainty, we generated a data set composed of 5000 samples containing measured variables. Here, the measured variables are D_d : diastolic diameter, ΔD distension, P_d and P_p diastolic and pulse pressure, respectively. IMT: intima-media thickness. Holzapfel-Gasser-Ogden models were fitted to single-exponential

diameter-pressure curves, determined for each sample of the generated data set. This yielded initial (INIT) realisations of mechanical characteristics, consisting of constitutive parameters and constituent load bearing parameters, that were subsequently used for uncertainty quantification and sensitivity analysis. The constitutive parameters are c_{elast} : elastin stiffness parameter; k_1 and k_2 : collagen stress scaling and stress curve shape parameters, respectively. The parameter R_i indicates the unstressed vessel inner radius and is an auxiliary model parameter. The load bearing parameter L_{coll} indicates the collagen load bearing as a percentage of the blood pressure (BP) load. *Right* assessing the relevance of uncertainty in load bearing parameters by simulating advanced glycation end product (AGE) breaker treatment using the model. We simulated AGE-breaker treatment by reducing parameters k_1 and k_2 equally with respect to their INIT best-fit values

(z) direction, respectively. The parameter c_{elast} is a constitutive (stiffness) parameter for elastin.

The SEF used for collagen (W_{coll}) is given by

$$W_{coll} = \frac{k_1}{k_2} \left[\exp \left[k_2 \left(\lambda_{\text{fibre}}^2 - 1 \right)^2 \right] - 1 \right], \quad (2)$$

where k_1 and k_2 are constitutive parameters and λ_{fibre} denotes fibre stretch, given by $\lambda_{\text{fibre}} = \sqrt{\cos^2(\beta_0)\lambda_{\theta\theta}^2 + \sin^2(\beta_0)\lambda_{zz}^2}$. This collagen SEF should only contribute when the fibres are extended (while collagen fibres cannot sustain compression; Holzapfel et al. 2000). The positive luminal arterial pressure used in all our simulations ensures that such condition is always met.

For incompressible materials, the local stress-strain behaviour can be calculated using the derivatives of the SEFs:

$$\sigma_n = -P_h + \lambda_n \frac{\partial W_{elast}}{\partial \lambda_n} + \lambda_n \frac{\partial W_{coll}}{\partial \lambda_n}, \quad (3)$$

with σ_n the Cauchy stress. The subscript n is rr for the radial direction, $\theta\theta$ for the circumferential direction and zz for the axial direction. The pressure P_h is the local hydrostatic pressure within the wall.

In W_{elast} and W_{coll} , the following parameters thus characterise the constitutive behaviour of elastin and collagen:

- c_{elast} : stiffness parameter of elastin, units of Pa.
- k_1 : stress scaling parameter of collagen, units of Pa.
- k_2 : collagen stress curve shape parameter, dimensionless.

Elastin acts physiologically as the predominant load bearer for low pressure loads, whereas collagen, which is modelled as an unstressed fibrous material for low pressure, starts bear-

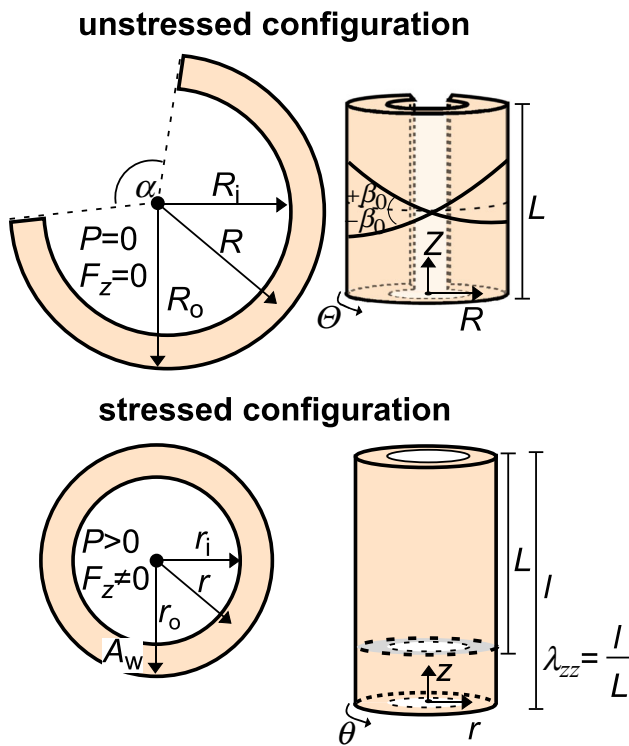


Fig. 2 Overview of unstressed (*top*) and stressed (*bottom*) configurations of an artery. *Top* P : internal pressure, F_z : reduced axial force, R : unstressed radius, R_i : unstressed inner radius, R_o : unstressed outer radius, α : opening angle, L : unstressed vessel length. In the unstressed configuration, we consider two families of helically orientated collagen fibres, with an angle $\pm\beta_0$ with respect to the circumferential direction. *Bottom* r : stressed radius, r_i : stressed inner radius, r_o : stressed outer radius, A_w : cross-sectional wall area in the stressed configuration, l : stressed vessel length, λ_{zz} : axial pre-stretch

ing load at higher pressures (Holzapfel and Ogden 2010; Watton et al. 2009; O'Rourke and Hashimoto 2007; Shadwick 1999). The fitted parameters should result in a relation that mimics this behaviour. To quantify collagen load bearing, we estimated L_{coll} , being the pressure load borne by collagen as a percentage of the total blood pressure load (see Appendix A1.4).

Based on the literature reports on excised human and animal carotid arteries, we assumed that the artery is subjected to an initial axial pre-stretch (λ_{zz} , Fig. 2) of 1.20 (Spronck et al. 2015a). The helix angle of the two families of collagen fibres in our model was assumed to be $\pm 35.3^\circ$ in the unstressed configuration (Fig. 2) (Avril et al. 2013). This angle was chosen from an analytical solution that for a thin-walled, fibre-reinforced tube results in a constant reduced axial force (F_z) over the cardiac cycle ($dF_z/dP = 0 \frac{N}{Pa}$) (Avril et al. 2013; Humphrey 2002; Takamizawa and Hayashi 1987; Weizsäcker et al. 1983; Van Loon 1976). Here, F_z is defined as the force applied in the axial direction additional to that generated by the pressure on the closed ends of the vessel (Holzapfel and Ogden 2010). Furthermore, in an earlier

study fitting a thick-walled two-fibre material model to experimental data from coronary arteries, an optimal fibre angle of 36° was found (van der Horst et al. 2012). Cross-sectional wall area (A_w , Fig. 2) was calculated from the diastolic outer diameter of the carotid (D_d) as well as IMT, using the relation given by

$$A_w = \pi \left(\frac{1}{4} D_d^2 - \left(\frac{1}{2} D_d - \text{IMT} \right)^2 \right). \quad (4)$$

To map from a cut, stress-free configuration of an artery, to an unloaded intact configuration, to a loaded configuration, we define two additional parameters (Fig. 2, Spronck et al. 2015a; Humphrey 2002; Holzapfel et al. 2002): the opening angle (α) and the unstressed inner vessel radius (R_i). The value for α was taken from the literature (100° , Spronck et al. 2015a). The parameter R_i was fitted using the constitutive model fitting routine (see below).

Residual stresses are accounted for by using the parameters λ_{zz} , α , and R_i to define the stretches in the loaded configuration with respect to the stress-free configuration, as described in Appendix A1. To obtain D - P and F_z - P relations, the following boundary value problem was considered. Assuming axisymmetry and neglecting torsion, acceleration forces, body forces and axial extension, the relevant components of the radial momentum balance are given by

$$\frac{\partial \sigma_{rr}}{\partial r} + \frac{\sigma_{rr} - \sigma_{\theta\theta}}{r} = 0. \quad (5)$$

Applying the boundary conditions $\sigma_{rr}(r_i) = -P$ and $\sigma_{rr}(r_o) = 0$, with r_i the vessel inner radius and r_o the vessel outer radius, the expression for lumen pressure is given by

$$P = \int_{r_i}^{r_o} \frac{\sigma_{\theta\theta} - \sigma_{rr}}{r} dr. \quad (6)$$

Reduced axial force is given by

$$F_z = \pi \int_{r_i}^{r_o} (2\sigma_{zz} - \sigma_{rr} - \sigma_{\theta\theta}) r dr. \quad (7)$$

2.2 Parameterisation

2.2.1 Clinical measurements

The measurement protocol and data used in the present study are elaborated by Holtackers et al. (2016). Briefly, twelve apparently healthy volunteers (22 ± 3 years, 6 males, 6 females) were recruited. The study was approved by the medical ethics committee of Maastricht University Medical Centre (Maastricht, the Netherlands), and written consent was obtained from all participants prior to enrolment.

Ultrasound (US) B-mode recordings were performed at the right common carotid artery (CCA) in the anterolateral plane, and obtained in triplicate. Diastolic blood pressure (P_d) and pulse pressure (P_p) were measured three times during the US imaging protocol using an oscillometric device (Omron 705IT; Omron Healthcare Europe, Hoofddorp, the Netherlands).

The US recordings were analysed to determine right CCA cyclic distension (i.e. diastolic–systolic diameter change, ΔD) and diastolic diameter (D_d). Because the echo tracking tool used (^{RF}QAS ; Esaote, Maastricht, the Netherlands) utilises the media–adventitia echoes of near and far walls, we assumed the measured diameter signal over time to reflect the CCA *outer* diameter (Spronck et al. 2015a). Furthermore, we obtained IMT at P_d using an automated software tool that reported good agreement with manual IMT methods (Willekes et al. 1999).

2.2.2 Generation of data set for constitutive modelling

For the present analysis, we obtained an initial data set consisting of group-averaged values for P_d , P_p , D_d , ΔD , and IMT (Fig. 1, left pane). Subsequently, uncertainties in the measured variables were accounted for by generating multiple samples within the uncertainty ranges of each measured metric. We assumed Gaussian distributed uncertainty domains for each measured variable M_i in \mathbf{M} , given by

$$M_i = \bar{M}_i \pm 1.96 \frac{SD_{intra, M_i}}{\sqrt{N_{rep}}}, \tag{8}$$

see also Table 1. Each sample consisted of a vector \mathbf{M} containing the following variables: $\mathbf{M} = [P_d, P_p, D_d, \Delta D, IMT]$.

Table 1 Overview of average values, intra-subject SDs, and uncertainty domains per measured variable

Parameter	Unit	Mean	Data of twelve subjects	
			Intra-subject SD	Uncertainty domain
P_d	mmHg	72	3.0	[69 ; 75]
P_p	mmHg	58	3.1	[54 ; 62]
D_d	mm	6.37	0.22	[6.12 ; 6.62]
ΔD	mm	0.789	0.035	[0.750 ; 0.829]
IMT	μm	539	40	[494 ; 584]

Intima–media thickness (IMT) was obtained at P_d . Intra-subject SD was determined using the method described in Bland and Altman (1996). The uncertainty domains of the measured variables were calculated using their respective mean and intra-subject SD values, see Eq. 8

Here, \bar{M}_i represents the average measured value of variable M_i and SD_{intra, M_i} represents the corresponding intra-subject standard deviation (i.e. indicating measurement error Bland and Altman 1996). In our data set, measurements were performed in triplicate (i.e. $N_{rep} = 3$) Holtackers et al. 2016. Samples were generated within the uncertainty domains of the measured variables, using Sobol’s low discrepancy series, implemented in the MATLAB Statistics and Machine Learning Toolbox function `sobolset` (MATLAB R2015a; The MathWorks, Natick, MA, USA) (Sobol 1967). This sampling method samples the uncertainty domains uniformly and was chosen as a “worst-case scenario.” To ensure adequate convergence of mechanical characteristics distributions, we generated 5000 samples. Systolic blood pressure (P_s) was calculated as $P_s = P_d + P_p$; systolic diameter (D_s) was calculated as $D_s = D_d + \Delta D$. The distributions of D_d , D_s , P_d , and P_s as well as IMT are shown in Fig. 3. The greater

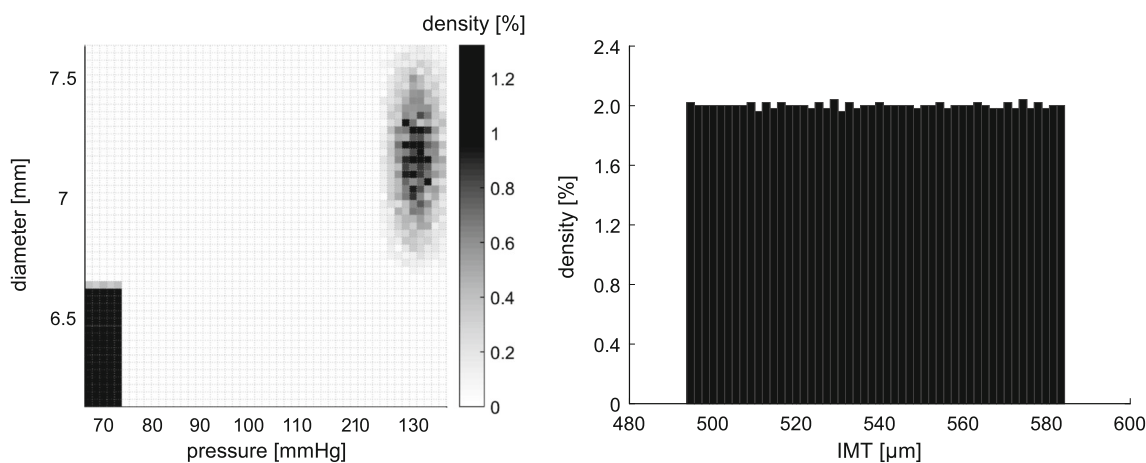


Fig. 3 Density plots displaying the distributions of the 5000 computer-generated samples for diastolic and systolic blood pressure and diameter (left), as well as intima–media thickness (right). Density of diastolic pressure and diameter as well as intima–media thickness samples is high. The greater amount of scattering of systolic diameter and pres-

sure samples arises from the fact that systolic blood pressure is defined as the sum of diastolic and pulse pressure, assumed independent. Similarly systolic diameter is defined as the sum of diastolic diameter and distension, also assumed independent

amount of scattering of systolic D and P data points compared to diastolic data points is caused by the fact that systolic blood pressure is defined as the sum of diastolic and pulse pressure. As diastolic and pulse pressure were assumed to be independent, their sum (systolic blood pressure) will have a larger spread than diastolic blood pressure alone. The larger spread in systolic diameter than in diastolic diameter has the same origin, as systolic diameter is defined as the sum of diastolic diameter and distension.

For each sample in the data set, the following single-exponential function was parameterised to obtain continuous D - P relations:

$$P(D) = P_d \exp \left[\gamma \left(\frac{D^2}{D_d^2} - 1 \right) \right]. \quad (9)$$

Here, D is a continuous variable describing vessel diameter and γ is a dimensionless non-linearity factor, which is calculated from systolic and diastolic blood pressures and diameters as described by Hayashi et al. (1980):

$$\gamma = \frac{\log \left(\frac{P_s}{P_d} \right)}{\frac{D_s^2}{D_d^2} - 1}. \quad (10)$$

2.2.3 Model fitting procedure

The constitutive model was fitted to the single-exponential curve, obtained for each sample \mathbf{M} of the data set. Model fitting was performed by variation of model parameters c_{elast} , k_1 , k_2 , and R_i (Fig. 1, left pane). Lower and upper bounds of all fitted parameters are given in Table 2.

For each sample in the data set, we assumed the single-exponential curve to be valid within the range $P \in \{P_{d,\text{sample}} - 15 \text{ mmHg}, P_{s,\text{sample}} + 15 \text{ mmHg}\}$ (Meinders and Hoeks 2004; Hayashi et al. 1980). In Fig. 3 (left), the distribution of $P_{d,\text{sample}}$ vs. $P_{s,\text{sample}}$ is displayed.

Fitting was performed using the trust-region reflective algorithm (Moré and Sorensen 1983), implemented in the MATLAB Optimization Toolbox function `lsqnonlin`, and initiated from 10 random start points in the parameter space using the MATLAB Global Optimization Toolbox function `MultiStart`. The same 10 start points were used for fitting

Table 2 Complete overview of lower and upper parameter bounds used for fitting the diameter–pressure data

Parameter	Unit	Lower bound	Upper bound
c_{elast}	kPa	1	400
k_1	kPa	0.1×10^{-3}	400
k_2	-	0	100
R_i	m	0.5×10^{-3}	10×10^{-3}

all samples. Throughout model fitting, we aimed to minimise the sum of squared differences between measured pressure from the single-exponential curve P_j and modelled $P_{\text{mod},j}$:

$$\epsilon_P = \frac{1}{n_P} \frac{1}{P_P^2} \sum_{j=1}^{n_P} (P_j - P_{\text{mod},j})^2, \quad (11)$$

where, for each sample, n_P is the number of fitting points and P_P is the pulse pressure.

As a physiological constraint, F_z was forced to remain constant at a target value defined $F_{z,\text{target}}$, with varying pressure. This assumption was based on experimental work performed by Van Loon (1976) and Weizsäcker et al. (1983), observing axial force to be nearly insensitive to changes in pressure for arteries inflated at their *in vivo* axial pre-stretch. We enforced this constraint by minimising the following expression:

$$\epsilon_{F_z} = \frac{1}{n_P} \frac{1}{F_{z,\text{target}}^2} \sum_{j=1}^{n_P} (F_{z,j} - F_{z,\text{target}})^2, \quad (12)$$

where $F_{z,\text{target}}$ was assumed to be equal to 0.5 N. This value was based on a study by Patel and Fry (1969) in excised, vertically suspended canine arteries that were extended by hanging weights from the bottom end of the artery. For the carotid artery to restore its *in vivo* length, a weight of 54 g was required, corresponding to an F_z of 0.5 N. The two weighted errors ϵ_P and ϵ_{F_z} are combined into the weighted total sum of squares (ϵ_T):

$$\epsilon_T = w_P \epsilon_P + w_{F_z} \epsilon_{F_z}, \quad (13)$$

where w_P and w_{F_z} are non-dimensional weighting factors. Here, we chose $w_P = 10$ and $w_{F_z} = 1$. The ϵ_P term was given a higher importance than the ϵ_{F_z} term, because of the absence of F_z measurements in our study and uncertainty in the assumed target value for F_z . The fitting error describing goodness of fit is expressed as a normalised root mean square error ($E_{\text{RMS},P}$ and E_{RMS,F_z}):

$$E_{\text{RMS},P} = 100\% \cdot \sqrt{\epsilon_P}, \quad \text{and} \quad (14)$$

$$E_{\text{RMS},F_z} = 100\% \cdot \sqrt{\epsilon_{F_z}}. \quad (15)$$

2.3 Simulations and analysis

2.3.1 Initial constitutive parameter estimation

The constitutive model was fitted to all 5000 samples of the generated data set using the procedure explained in the previous section. This yielded 5000 initial constitutive model realisations (i.e. termed INIT).

2.3.2 Uncertainty quantification and sensitivity analysis

All constitutive model realisations together yield insight in the distribution of the mechanical characteristics that results from the presence of measurement uncertainty. This distribution of mechanical characteristics was therefore used to quantify the uncertainty in constitutive parameters (i.e. the fitted parameters c_{elast} , k_1 , and k_2), as well as collagen load bearing parameters (i.e. the outcome parameter L_{coll} at various blood pressure levels, Fig. 1, left pane). We used kernel density estimation (KDE) to visualise the distributions of constitutive parameters and load bearing parameters. KDE estimates the probability density function, which in this context implies the probability density of finding a certain value of a constitutive parameter or load bearing value (Silverman 1986). Furthermore, we quantified spread in parameters using the median and the 25th to 75th percentile confidence interval ($\text{PCI}_{25 \rightarrow 75}$). Calculating the $\text{PCI}_{25 \rightarrow 75}$ comes at hand when assessing spread of skewed distributions.

Sensitivity analysis (SA) was subsequently used to apportion uncertainty in the model-predicted mechanical characteristics to uncertainty in specific measured variables, or their interactions (Huberts et al. 2014). A global variance-based SA was performed using regression-based adaptive generalised polynomial chaos expansion (agPCE), as detailed in Quicken et al. (2016). The agPCE method captures the relation between mechanical characteristics (X_i) and measured variables (M_i) by means of an adaptively constructed finite polynomial expansion f_{agPCE} :

$$X_i = f^{X_i}(\mathbf{M}) \approx f_{\text{agPCE}}^{X_i}(\mathbf{M}). \quad (16)$$

Here, \mathbf{X} contains the mechanical characteristics, i.e. $\mathbf{X} = [c_{\text{elast}}, k_1, k_2, L_{\text{coll}}]$.

Furthermore, $\mathbf{M} = [M_1, M_2, \dots, M_{N_{\text{vars}}}] = [P_d, P_p, D_d, \Delta D, \text{IMT}]$, and N_{vars} is the number of measured variables. Such a polynomial expansion provides a meta-model of the mechanical characteristics estimation method. After constructing the meta-model, the value of the leave-one-out cross-validation coefficient (Q^2) was computed. Coefficient Q^2 , ranging between a value of 0 and 1, is a quality measure of the meta-model, indicating its predictive properties (Sudret 2015). Throughout this study, we assumed $Q^2 > 0.99$ to indicate an appropriate meta-model.

From the meta-model, the variance of a mechanical characteristic (a measure of its uncertainty) can be computed. The following sensitivity metrics were computed:

- *Main sensitivity indices* The main sensitivity index (S_i) of measured variable M_i represents the expected reduction in uncertainty of the mechanical characteristic if M_i were known exactly. Assessment of S_i determines which measured variables are most rewarding to be measured

more accurately to reduce model output uncertainty (i.e. parameter prioritisation) (Saltelli et al. 2008).

- *Total sensitivity indices* The total sensitivity index (S_T) of M_i represents the expected uncertainty in the mechanical characteristic that would remain if all other measured variables except M_i were known exactly. Assessment of S_T determines which measured variables could potentially be fixed within their uncertainty domain (i.e. parameter fixing) (Saltelli et al. 2008).

The contribution of each measured variable to total uncertainty in estimating mechanical characteristics can be illustrated as the segments of a disc (Fig. 1). Total uncertainty may be apportioned to single measured variables but may also arise from interaction between measured variables (Fig. 1). Moreover, significant interaction effects are indicated by large differences between total sensitivity indices and main sensitivity indices (Sudret 2008).

2.3.3 Simulating the effect of AGE-breaker vascular drugs

AGE-breaker treatment was simulated using the INIT realisations as take-off points (Fig. 1, right pane). We explicitly assumed that a reduction in cross-link density can be represented in the model by reducing parameters k_1 and k_2 . The rationale of reducing k_1 and k_2 is based on previous work measuring the stress–strain response of collagen tissue at multiple levels of cross-linking (Kayed et al. 2015; Fratzl 2008). In their work, it was observed that a decrease in cross-link density results in (1) a decrease in fibre stiffness at low amounts of strain and (2) a decrease in the non-linearity of the fibre stress–strain response (Kayed et al. 2015; Fratzl 2008). In our analysis, k_1 and k_2 were equally reduced by 40% of their initial best-fit value yielding the $k_1 \downarrow, k_2 \downarrow$ realisations (Fig. 1, right pane). All other constitutive model parameters were assumed to remain unchanged.

3 Results

3.1 Representative example of a fitted constitutive model

A representative example of a model-based D - P and F_z - P relationship obtained by model fitting a sample within the virtual data set is depicted in Fig. 4. The best-fit constitutive parameters for this representative sample were $c_{\text{elast}} = 40.1$ kPa, $k_1 = 6.9$ kPa and $k_2 = 8.5$. Collagen load bearing (L_{coll}) increased monotonically with blood pressure from 0.6% at diastolic blood pressure (P_d), to 10.2% at mean arterial pressure (P_m), up to 25.0% at systolic blood pressure (P_s), respectively. The slope of the plotted curves (dD/dP) is a measure of vascular compliance. Low vascular compliance corresponds to high vascular stiffness and vice versa.

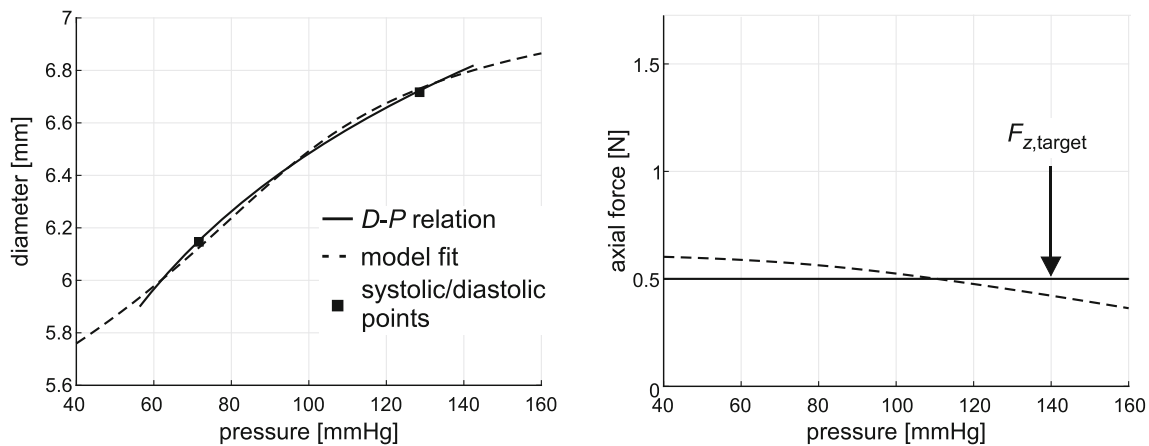


Fig. 4 Representative example of the model-predicted diameter–pressure (D - P) curve and the reduced axial force–pressure (F_z - P) curve (dashed lines) as well as the group-averaged data fitted upon (solid lines). The difference between measured and model-predicted pressure was minimised over the pressure fitting range (i.e. $P_d + 15$ mmHg to

$P_s + 15$ mmHg), whereas reduced axial force was fitted to an assumed target value of 0.5 N ($F_{z,target}$, respectively). Values of fitted parameters were $c_{elast} = 40.1$ kPa, $k_1 = 6.9$ kPa and $k_2 = 8.5$. Fit errors, describing the goodness of fit were $E_{RMS,P} = 0.020\%$ and $E_{RMS,F_z} = 16\%$, respectively

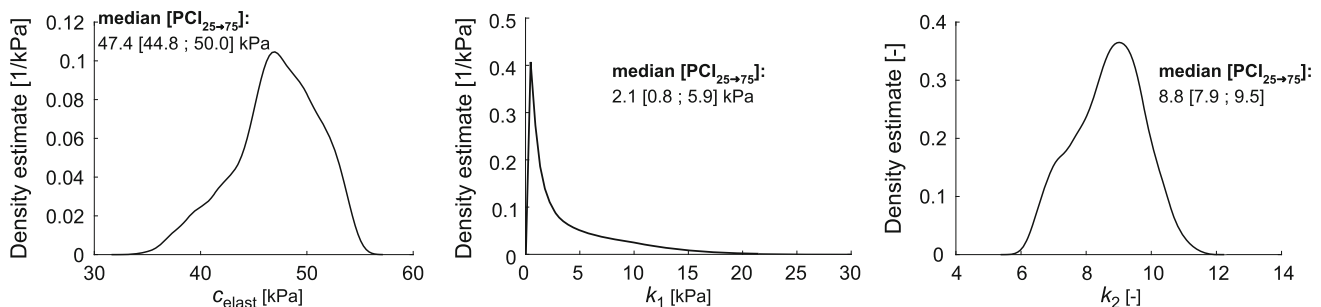


Fig. 5 Kernel density estimation (KDE) describing the distributions of fitted constitutive parameters (c_{elast} , k_1 , and k_2). Distributions of parameters were quantified using the median and the 25th to 75th percentile confidence interval ($PCI_{25 \rightarrow 75}$), respectively

The model fit (dashed lines, Fig. 4) shows sigmoidal D - P behaviour over a 40 to 160 mmHg pressure range, suggesting low compliance for the lower part of pressure range followed by higher compliance in the physiological pressure range and again lower compliance for the upper part of the pressure range. Furthermore, there is some deviation between the model-based F_z - P curve and the assumed (pressure-independent) target value of 0.5 N (Fig. 4).

3.2 Uncertainty quantification and sensitivity analysis

The distributions of the fitted constitutive parameters are shown in Fig. 5. Best-fit parameter values for elastin stiffness (c_{elast}) were 47.4 [44.8 ; 50.0] (median [$PCI_{25 \rightarrow 75}$]). For collagen parameters, best-fit parameter values were 2.1 [0.8 ; 5.9] kPa for k_1 , and 8.8 [7.9 ; 9.5] for k_2 , respectively.

In Fig. 6, distributions of collagen load bearing parameters (L_{coll}) are given at three blood pressure levels (P_d , P_m , and P_s , respectively). Note that $L_{coll} = 0\%$ indicates that blood pressure load is fully borne by elastin, whereas $L_{coll} = 100\%$

indicates that blood pressure load is fully borne by collagen. For the initial constitutive model realisations (INIT), we found L_{coll} equal to 1.5% at P_d , 3.1% at P_m , and 16.7% at P_s (medians, respectively). As shown in Fig. 6, the 25th to 75th percentile confidence interval for L_{coll} at P_d as well as P_s were large ([0.6 ; 4.5]% and [12.7 ; 24.0]%, respectively), indicating large uncertainty in model predictions of constituent load bearing.

A full overview of main and total sensitivity indices is given in Tables 3 and 4. In general, distension and IMT were most rewarding to be measured more reliably. For the constitutive parameters c_{elast} and k_1 , this is illustrated by main sensitivity indices (S_i) between 0.62 and 0.90 for distension and 0.31 for IMT (Table 3).

For collagen parameter k_2 , distension and diastolic diameter are most influential (Table 3). Moreover, pulse pressure has some influence, indicated by an S_i of 0.10 (Table 3). For collagen load bearing (L_{coll}), distension was the most important measured variable, indicated by S_i between 0.87 and 0.90 (Table 4). The S_i s of the other measured vari-

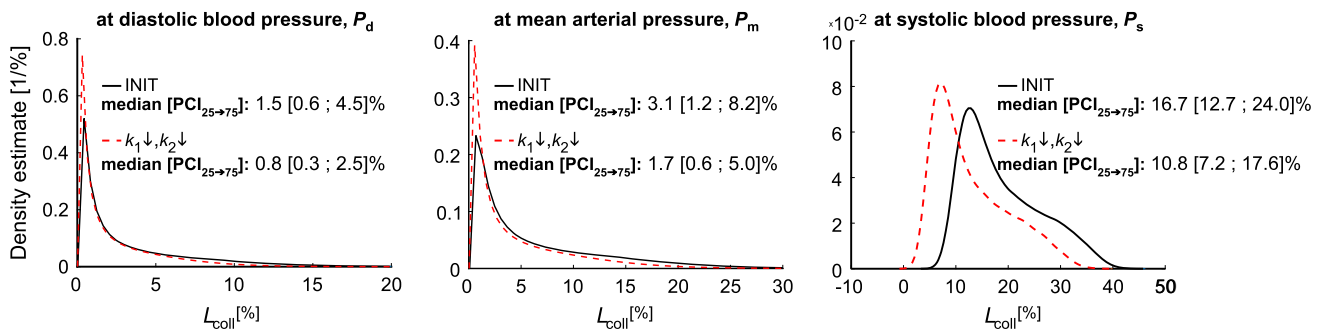


Fig. 6 Kernel density estimation (KDE) describing the distribution of collagen load bearing characteristic (L_{coll}). *Black line*: KDEs for initial constitutive model realisations (INIT). *Red dashed line*: KDEs for model with decreased k_1 and k_2 ($k_1 \downarrow, k_2 \downarrow$). KDEs were calculated at

three blood pressure levels; diastolic blood pressure (P_d), mean arterial pressure (P_m) and systolic blood pressure (P_s). Distributions of parameters were quantified using the median and the 25th to 75th percentile confidence interval (PCI_{25→75}), respectively

Table 3 Main (S_i) and total (S_T) sensitivity indices for constitutive parameters c_{elast} , k_1 and k_2

Measured variable	Symbol	Constitutive parameter					
		c_{elast}		k_1		k_2	
		S_i	S_T	S_i	S_T	S_i	S_T
Diastolic blood pressure	P_d	0.012	0.014	0.00060	0.0011	0.052	0.056
Pulse pressure	P_p	0.0018	0.021	0.027	0.041	0.10	0.12
Diastolic diameter	D_d	0.0060	0.036	0.033	0.047	0.29	0.32
Distension	ΔD	0.62	0.67	0.90	0.93	0.50	0.54
Intima–media thickness	IMT	0.31	0.31	0.0083	0.015	0.00083	0.00083

Sensitivity indices larger than 0.10 are indicated in bold. The coefficient Q^2 , indicating the accuracy of the meta-model, was 0.997, 0.998, and 0.998 for c_{elast} , k_1 , and k_2 , respectively

Table 4 Main (S_i) and total (S_T) sensitivity indices for collagen load bearing parameters (L_{coll}) at three blood pressure levels: diastolic, mean, and systolic blood pressure (i.e. P_d , P_m and P_s , respectively)

Measured variable	Symbol	Load bearing parameter					
		L_{coll} at P_d		L_{coll} at P_m		L_{coll} at P_s	
		S_i	S_T	S_i	S_T	S_i	S_T
Diastolic blood pressure	P_d	0.00043	0.00098	0.00073	0.0016	0.0019	0.0027
Pulse pressure	P_p	0.021	0.035	0.023	0.035	0.052	0.054
Diastolic diameter	D_d	0.036	0.058	0.041	0.059	0.064	0.067
Distension	ΔD	0.90	0.94	0.90	0.93	0.87	0.88
Intima–media thickness	IMT	0.0028	0.0049	0.0031	0.0046	0.0031	0.0048

Sensitivity indices larger than 0.10 are indicated in bold. The coefficient Q^2 , indicating the accuracy of the meta-model, was 0.993, 0.995, and 0.999 for diastolic (P_d), mean (P_m), and systolic blood pressure (P_s), respectively

ables were smaller than 0.06, indicating low influence (Table 4). Reducing uncertainty of blood pressure measurements appears of negligible importance in reducing uncertainty in estimating c_{elast} , k_1 , and L_{coll} , indicated by an $S_i < 0.06$ (Tables 3 and 4). Moreover, total sensitivity indices (S_T) for diastolic blood pressure and pulse pressure were smaller than 0.12, suggesting these variables could be fixed in their uncertainty domain. For all measured variables, differences between main and total sensitivity indices were minor, i.e. $S_T - S_i$ was smaller than 0.10 (Tables 3 and 4). This indicates that the contribution of interaction terms between measured

variables to the total variance was negligible (Saltelli et al. 2008).

3.3 Model-based assessment of vascular drug therapies

Figure 7 shows the effect of AGE-breaker treatment (simulated by $k_1 \downarrow, k_2 \downarrow$) on the model-predicted $D-P$ curve, as well as on area compliance (C_A). Here, the average $D-P$ curves, originating on the one hand from the initial best-fit constitutive parameters (INIT, black line), and on the other hand following reduction of k_1 and k_2 ($k_1 \downarrow, k_2 \downarrow$, red dashed

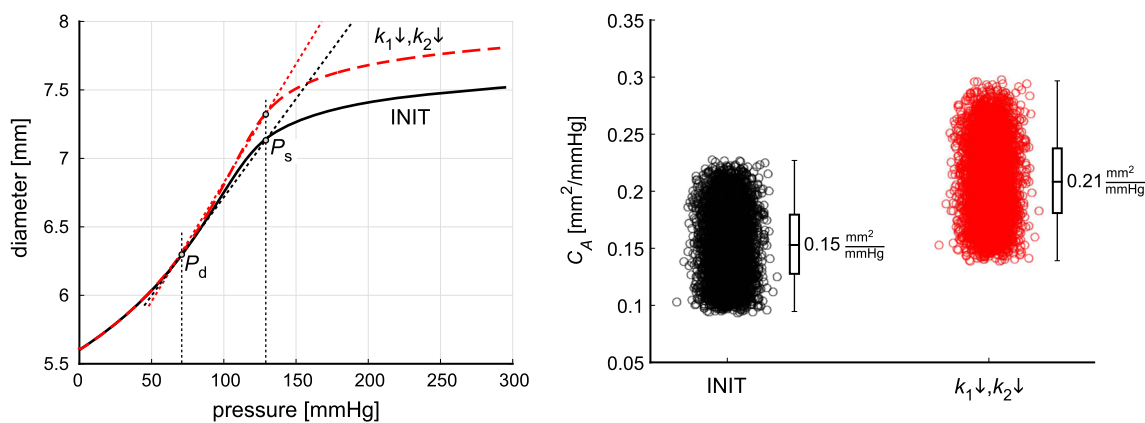


Fig. 7 Left pane: Reducing collagen parameters k_1 and k_2 with 40% (i.e. $k_1 \downarrow, k_2 \downarrow$), caused a left-upward shift in the average diameter–pressure (D - P) relation. Tangent lines (dotted lines) from the diastolic D - P point to the systolic D - P point indicate area compliance. Right pane: Simulating $k_1 \downarrow, k_2 \downarrow$ caused area compliance (C_A) to increase

line), are shown. Moreover, C_A is shown in the right pane for all INIT realisations (black circles) and the $k_1 \downarrow, k_2 \downarrow$ realisations (red circles). Area compliance was calculated using $C_A = (A_s - A_d) / (P_s - P_d)$, with $A_s = \pi (D_d + \Delta D)^2 / 4$ and $A_d = \pi D_d^2 / 4$, respectively. Simulating $k_1 \downarrow, k_2 \downarrow$ caused a left-upward shift of the group-averaged D - P curve, as well as a 40% increase in C_A (Fig. 7). In Fig. 6, distributions of L_{coll} for the $k_1 \downarrow, k_2 \downarrow$ realisations (red dashed curves) are shown. We found L_{coll} to equal 0.8 [0.3 ; 2.5]% at P_d , 1.7 [0.6 ; 5.0]% at P_m , and 10.8 [7.2 ; 17.6]% at P_s (median [PCI_{25→75}]). As compared to the INIT realisations, spread in L_{coll} was lower for $k_1 \downarrow, k_2 \downarrow$ realisations (Fig. 6).

4 Discussion

Computational models of arterial wall mechanics could be valuable for predicting effects of vascular drug therapies on individual arterial wall constituents. The aim of this study was (1) to quantify how measurement noise propagates into uncertainty of the model predictions and (2) to pinpoint the measurements responsible for the largest spread in mechanical characteristics. The relevance of the model output uncertainty was assessed by simulating the effects of vascular drug treatment on constituent load bearing. To our knowledge, this is the first study to perform rigorous uncertainty quantification and sensitivity analysis, assessing the influence of measurement noise in clinical arterial pressure and diameter measurements on constitutive model predictions.

The present study demonstrates that the clinical usefulness of estimating mechanical characteristics of the carotid artery using a constitutive model is hampered by measurement uncertainty. Using sensitivity analysis, we pinpointed that the majority of uncertainty in mechanical characteristics

is caused by uncertainty in measurements of distension and IMT. from 0.15 mm²/mmHg to 0.21 mm²/mmHg, respectively. For each INIT and $k_1 \downarrow, k_2 \downarrow$ realisation, area compliance was calculated using $C_A = (A_s - A_d) / (P_s - P_d)$, with $A_s = \pi (D_d + \Delta D)^2 / 4$ and $A_d = \pi D_d^2 / 4$, respectively

is caused by uncertainty in measurements of distension and IMT.

4.1 Model fitting and parameter estimation

Model fitting was performed on single-exponential diameter–pressure curves calculated from diastolic and systolic diameters and pressures. The assumption of a markedly exponential diameter–pressure curve in the physiological (i.e. diastolic to systolic) pressure range was reported in earlier works by Hayashi et al. (1980) and Meinders and Hoeks (2004). At a wider pressure range (i.e. 40–160 mmHg), a representative constitutive model realisation suggested sigmoidal diameter–pressure behaviour (Fig. 4). Such sigmoidal behaviour was also observed in *in vitro* studies, performing inflation tests on human aortic segments and rat carotid arteries (Fridez et al. 2003; Langewouters et al. 1986).

In the present study, best-fit constitutive parameter values for elastin stiffness (i.e. 47.4 [44.8 ; 50.0] kPa) were in agreement to those found for cadaveric carotid arteries, reporting values between 20 and 60 kPa (Sáez et al. 2014; Sommer and Holzapfel 2012). Moreover, values for collagen parameter k_2 were well within ranges found in earlier studies (Sáez et al. 2014; Sommer and Holzapfel 2012). We found a large spread for constitutive parameter k_1 , governing collagen stiffness, i.e. median [PCI_{25→75}] of 2.1 [0.8 ; 5.9] kPa. Previous *in vitro* studies found k_1 values ranging from 2.9 to 99.9 kPa, respectively (Sommer and Holzapfel 2012). Therefore, our findings for k_1 are on the low end to those found in the aforementioned studies. It has been pointed out that appropriate choices of both k_1 and k_2 ensure collagen to virtually not bear load at very low amounts of stretch (i.e. at sub-physiological pressure loads), whereas it will become the dominant load bearer at high amounts of stretch (Holzapfel et al. 2000). In the present study, and in *in vivo* studies *per se*, diame-

Table 5 Effect of increasing the number of repeated clinical measurements (N_{rep}) on collagen load bearing parameters (L_{coll}) as predicted using the initial constitutive model realisations

N_{rep}	L_{coll} at P_d		L_{coll} at P_m		L_{coll} at P_s	
	Median [%]	PCI _{25→75} [%]	Median [%]	PCI _{25→75} [%]	Median [%]	PCI _{25→75} [%]
3	1.5	[0.6 ; 4.5]	3.1	[1.2 ; 8.2]	16.7	[12.7 ; 24.0]
5	1.5	[0.7 ; 3.5]	3.0	[1.4 ; 6.7]	16.5	[13.2 ; 21.8]
10	1.5	[0.9 ; 2.7]	3.0	[1.8 ; 5.3]	16.5	[14.0 ; 19.9]

PCI_{25→75}: 25th to 75th percentile confidence interval, P_d : diastolic blood pressure, P_m : mean blood pressure, and P_s : systolic blood pressure

ter and pressure measurements at these very low pressures are unavailable, making robust estimation of model parameters (particularly k_1) cumbersome, as illustrated by our findings.

4.2 Sensitivity analysis

Sensitivity analysis indicated that the most important contributors to uncertainty in c_{elast} are both the variables measured by ultrasound (i.e. distension and IMT), whereas uncertainty in collagen parameter k_1 was primarily caused by measurement uncertainty of distension. Although our model-based approach still requires blood pressure to be measured, improving the precision of distension and wall thickness measurements clearly appears to be most rewarding. Recent technological advances in vascular imaging, including plane wave ultrasound and image-reconstruction algorithms, could reduce the measurement noise of a single ultrasound measurement (Besson et al. 2016). More practically, uncertainty in mechanical characteristics could be reduced by increasing the number of repeated measurements (N_{rep} , Eq. 8).

4.3 Decreasing measurement uncertainty by increasing the number of repeated measurements

We evaluated to which extent increasing N_{rep} , for all measured variables displayed in Table 1, influenced uncertainty in collagen load bearing parameters. Results indicate that increasing the number of repeated measurements from 3 to 10 decreases the spread in L_{coll} by $\sim 50\%$ (i.e. reducing the 25th to 75th percentile confidence interval at systolic blood pressure from [12.7 ; 24.0]% to [14.0 ; 19.9]%, Table 5). Based on the results of our sensitivity analysis, increasing the number repetitions of ultrasound measurements appears most rewarding in reducing uncertainty in collagen load bearing parameters.

4.4 Model-based assessment of vascular drug therapies

AGE-breaking vascular drug therapy was simulated by changing constitutive model parameters governing collagen behaviour (i.e. parameters k_1 and k_2). We chose to reduce

collagen stress scaling parameter k_1 , as well as collagen stress curve shape parameter k_2 by 40% of their initial best-fit values. Consequently, the modelled collagen becomes incrementally less stiff at low amounts of strain, but will also stiffen “later” (i.e. at higher amounts of strain), compared to when the initial parameters would be used (Fig. 6). This shift in stress–strain behaviour with decreasing cross-link densities was measured also in collagenous tissue such as the pericardium (Kayed et al. 2015; Fratzl 2008). Reducing constitutive parameters k_1 and k_2 by 40% resulted in a model-predicted area compliance increase from 0.15 mm²/mmHg to 0.21 mm²/mmHg (Fig. 7). This observed 40% increase in area compliance is in agreement with in vitro measurements performed in rat carotid arteries, following AGE-breaker treatment (Wolffenbuttel et al. 1998). Furthermore, collagen load bearing is reduced, with the load transferred to elastin instead (Figs. 6 and 7). The median reduction of collagen load bearing was 1%, 2%, and 6% at diastolic, mean, and systolic blood pressures (Fig. 6). However, the reduction in collagen load bearing was exceeded by the initial spread in collagen load bearing. This is illustrated by the reduction in collagen load bearing at systolic blood pressure (6%, respectively, Fig. 6), which is much smaller compared to the 25th to 75th percentile confidence interval ranging between 12.7 and 24.0%, respectively (Fig. 6). In other words, measurement of the benefit of a cross-link breaker on arterial compliance may be easily concealed by uncertainties in the estimation of the effects, given the impact of noise on model output.

4.5 Limitations

Unfortunately, no actual distensibility measurements, acquired before and during AGE-breaker treatment, were available in this study. Consequently, we had to resort to simulating AGE-breaker treatment using our constitutive model. This was achieved by changing constitutive parameters governing collagen behaviour, reproducing results from an earlier AGE-breaker intervention study (Wolffenbuttel et al. 1998). The Holzapfel-Gasser-Ogden model we used-neglecting active smooth muscle response and containing only three parameters to characterise elastin and collagen behaviour-was chosen as a pragmatic simplification of the actual arterial biomechanical behaviour. Furthermore, our

model neglects the dispersion of collagen fibre orientation in the adventitia (Gasser et al. 2006). We are aware that more elaborate models exist describing the influence of collagen cross-links on the stress–strain behaviour of an artery more directly. For example, in the work of Sáez et al. (2014), a cross-linking degree parameter was introduced which includes cross-links behaviour between the main collagen fibres. However, using such a model requires estimating one extra model parameter. To ensure unique parameter values, this would require more clinical data to be measured, which might not be possible in *in vivo* situations. Of note, parameter values in the current study were highly similar, indicated by the fact that the best-fit constitutive parameter values—for each of the 10 random starting points—were highly similar.

In our model, not all combinations of c_{elast} , k_1 , and k_2 yield physiological behaviour. However, the adjustment (fitting) of these parameters ensures that eventually their combination does yield physiological behaviour. The parameter c_{elast} can be physiologically interpreted as the stiffness of the arterial elastin. All fitted values for this parameter ranged from 35 to 55 kPa, which corresponds to previous literature (Sommer and Holzapfel 2012). For k_1 and k_2 , no separate interpretation can be made in terms of physiology. Nevertheless, the fitted combinations of k_1 and k_2 yielded physiologically realistic mechanical behaviour which, given that the elastin model was plausibly parameterised, corresponds to realistic collagen behaviour.

The global variance-based sensitivity analysis method used distinguishes from more commonly used local methods by taking into account the entire distribution of measured variables, being model free, and assessing interaction between measured variables (Borgonovo and Plischke 2016; Quicken et al. 2016; Sudret 2015). However, it assumes on the one hand statistical independence between measured variables and on the other hand that variance is an adequate metric for model uncertainty. The latter assumption becomes questionable for skewed distributions of parameters, i.e. as present in the distributions of parameters k_1 and L_{coll} at P_d and P_m , respectively (Figs. 5 and 7). A solution to this problem could be to use moment-independent sensitivity methods instead (Borgonovo and Plischke 2016). To this end, Borgonovo (2007) evaluated an alternative sensitivity metric that, instead of being computed using the variance of the model uncertainty distribution, considers this distribution as a whole. In their paper, it was concluded that sensitivity indices of both methods (1) show discrepancies between influential measured variables, but (2) agree in distinguishing non-influential from influential measured variables (Borgonovo 2007). Based on these findings, we believe that utilising the variance-based sensitivity analysis as proposed by Quicken et al. (2016) in this study is justified.

4.6 Conclusion

This study shows that *in vivo* assessment of arterial wall mechanics using a constitutive model is hampered by large model uncertainty. We quantified model uncertainty in constitutive parameters (i.e. c_{elast} , k_1 , and k_2 , respectively), and collagen load bearing parameters, at various blood pressures (L_{coll}). Our simulation of vascular drug therapy suggested a reduction of collagen load bearing of 6-percentage points, at systolic blood pressure. This reduction is 3–4 times lower compared to its uncertainty. Therefore, model output uncertainty could conceal potential effects of vascular drugs. Sensitivity analysis revealed that estimation of mechanical characteristics would benefit most from increasing the precision of measurements of arterial diameter, distension, and wall thickness. Whereas the potential for improving the precision of, for example, a single ultrasound measure is practically limited, the effective precision of ultrasound measurements could be improved by increasing the number of repeated measurements.

Funding This study was funded by a Kootstra Talent Fellowship awarded to M.H.G. Heusinkveld by Maastricht University Medical Centre, S. Quicken is paid by Chemelot InSciTe, R.J. Holtackers received funding from Stichting de Weijerhorst, and B. Spronck was funded by an Endeavour Research Fellowship from the Australian government.

Compliance with ethical standards

Conflict of Interest The authors declare that they have no conflict of interest.

Open Access This article is distributed under the terms of the Creative Commons Attribution 4.0 International License (<http://creativecommons.org/licenses/by/4.0/>), which permits unrestricted use, distribution, and reproduction in any medium, provided you give appropriate credit to the original author(s) and the source, provide a link to the Creative Commons license, and indicate if changes were made.

A1 Appendix: Constitutive model

A1.1 Constitutive relations

Under the assumptions that (1) elastin and collagen act in parallel in terms of mechanical load bearing, (2) the vessel wall is incompressible, and (3) deformation occurs only along the principal axes, the constituent-specific strain energy functions (Eqs. 1 and 2) were cast into a relation describing local Cauchy stress:

$$\sigma_n = -P_h + \lambda_n \frac{\partial W_{\text{elast}}}{\partial \lambda_n} + \lambda_n \frac{\partial W_{\text{coll}}}{\partial \lambda_n}, \quad (\text{A1})$$

The subscript n is rr for the radial direction, $\theta\theta$ for the circumferential direction and zz for the axial direction. This

results in the following expressions for σ_{rr} , $\sigma_{\theta\theta}$ and σ_{zz} :

$$\begin{aligned} \sigma_{rr} &= -P_h + 2\lambda_{rr}^2 c_{\text{elast}} , \\ \sigma_{\theta\theta} &= -P_h + 2\lambda_{\theta\theta}^2 c_{\text{elast}} \\ &\quad + 4k_1 \lambda_{\theta\theta}^2 (\lambda_{\text{fibre}}^2 - 1) \cos^2(\beta_0) \left(\exp \left[k_2 \left(\lambda_{\text{fibre}}^2 - 1 \right)^2 \right] \right) , \\ \text{and} \\ \sigma_{zz} &= -P_h + 2\lambda_{zz}^2 c_{\text{elast}} \\ &\quad + 4k_1 \lambda_{zz}^2 (\lambda_{\text{fibre}}^2 - 1) \sin^2(\beta_0) \left(\exp \left[k_2 \left(\lambda_{\text{fibre}}^2 - 1 \right)^2 \right] \right) \end{aligned} \tag{A2}$$

with P_h the local hydrostatic pressure within the wall, λ_{fibre} the fibre stretch given by $\lambda_{\text{fibre}} = \sqrt{\cos^2(\beta_0)\lambda_{\theta\theta}^2 + \sin^2(\beta_0)\lambda_{zz}^2}$, β_0 the fibre helix angle, c_{elast} the constitutive (stiffness) parameter of elastin, and k_1 and k_2 stiffness parameters of collagen, respectively.

A1.2 Constitutive framework

We distinguished between the unstressed and stressed states of an artery (Fig. 2). Under the assumption of an incompressible wall tissue, a mapping of coordinates (r, θ, z) of the deformed, stressed configuration to coordinates (R, Θ, Z) of the unstressed configuration is given by:

$$r(R) = \sqrt{r_o^2 - \frac{R_o^2 - R^2}{\lambda_{zz} k_\alpha}} , \quad \theta = k_\alpha \Theta , \quad \text{and} \quad z = \frac{l}{L} Z , \tag{A3}$$

where R_o and r_o are the outer radii of respectively the unstressed and stressed configuration (Fig. 2). The parameter k_α is defined as $k_\alpha = \frac{2\pi}{2\pi - \alpha}$, with α the opening angle (Fig. 2). L and l are vessel length of the unstressed and stressed configuration defining the initial pre-stretch of an artery λ_{zz} (Fig. 2). The principal stretch ratios $(\lambda_{rr}, \lambda_{\theta\theta}, \lambda_{zz})$ with respect to the unstressed configuration are:

$$\lambda_{rr} = \frac{R}{r k_\alpha \lambda_{zz}} , \quad \lambda_{\theta\theta} = \frac{k_\alpha r}{R} , \quad \text{and} \quad \lambda_{zz} = \frac{l}{L} . \tag{A4}$$

Inner and outer radii (r_i and r_o , respectively) in the stressed configuration can be written as follows:

$$r_i = \frac{\lambda_{\theta\theta} R_i}{k_\alpha} \quad \text{and} \quad r_o = \sqrt{\frac{A_w}{\pi} + r_i^2} , \tag{A5}$$

where A_w is the cross-sectional wall area in the stressed configuration (Fig. 2). In practice, A_w can be determined by measuring IMT and vessel diameter using ultrasonography (Hoeks et al. 1999). We furthermore assumed $\lambda_{zz} = 1.20$, $\alpha = 100^\circ$, and $\beta_0 = 35.3^\circ$.

A1.3 Balance equations

Conservation of momentum is given by

$$\nabla \cdot \boldsymbol{\sigma} = \mathbf{0} , \tag{A6}$$

with ∇ the spatial gradient operator. Assuming axisymmetry and neglecting torsion, acceleration forces, body forces and axial extension, Eq. A6 reduces to

$$\frac{\partial \sigma_{rr}}{\partial r} + \frac{\sigma_{rr} - \sigma_{\theta\theta}}{r} = 0 . \tag{A7}$$

Applying the boundary conditions $\sigma_{rr}(r_i) = -P$ and $\sigma_{rr}(r_o) = 0$, the expression for lumen pressure (P) is given by

$$P = \int_{r_i}^{r_o} \frac{\sigma_{\theta\theta} - \sigma_{rr}}{r} dr . \tag{A8}$$

Reduced axial force is given by

$$F_z = \pi \int_{r_i}^{r_o} (2\sigma_{zz} - \sigma_{rr} - \sigma_{\theta\theta}) r dr . \tag{A9}$$

A1.4 Calculating collagen load bearing parameters

We calculated collagen load bearing (L_{coll}) at three blood pressure levels: diastolic, mean and systolic blood pressure (i.e. P_d , P_m , and P_s , respectively). Mean blood pressure (P_m) was calculated as $\frac{1}{3} P_s + \frac{2}{3} P_d$. Using Eq. A2, the expression for L_{coll} is given by

$$L_{\text{coll}} = \int_{r_i}^{r_o} \frac{\tau_{\theta\theta, \text{coll}}}{\sigma_{\theta\theta} - \sigma_{rr}} dr \Big|_{P \in \{P_d, P_m, P_s\}} \cdot 100\% , \tag{A10}$$

with $\tau_{\theta\theta, \text{coll}}$ the circumferential stress borne by collagen, given by

$$\tau_{\theta\theta, \text{coll}} = \lambda_{\theta\theta} \frac{\partial W_{\text{coll}}}{\partial \lambda_{\theta\theta}} . \tag{A11}$$

References

Avril S, Badel P, Gabr M, Sutton MA, Lessner SM (2013) Biomechanics of porcine renal arteries and role of axial stretch. *J Biomech Eng* 135(8):081007

Besson A, Zhang M, Varray F, Liebgott H, Friboulet D, Wiaux Y, Thiran JP, Carrillo RE, Bernard O (2016) A sparse reconstruction framework for fourier-based plane-wave imaging. *IEEE Trans Ultrason Ferroelectr Freq Control* 63(12):2092–2106

Bland JM, Altman DG (1996) Statistics notes: measurement error. *BMJ* 313(7059):744

Borgonovo E (2007) A new uncertainty importance measure. *Reliab Eng Syst Saf* 92(6):771–784

- Borgonovo E, Plischke E (2016) Sensitivity analysis: a review of recent advances. *Eur J Oper Res* 248(3):869–887
- Brownlee MMD (1995) Advanced protein glycosylation in diabetes and aging. *Annu Rev Med* 46(1):223–234
- Engelen L, Stehouwer C, Schalkwijk C (2013) Current therapeutic interventions in the glycation pathway: evidence from clinical studies. *Diabetes Obes Metab* 15(8):677–689
- Fratzl P (2008) Collagen: structure and mechanics. Springer Science & Business Media, Berlin
- Fridez P, Zulliger M, Bobard F, Montorzi G, Miyazaki H, Hayashi K, Stergiopoulos N (2003) Geometrical, functional, and histomorphometric adaptation of rat carotid artery in induced hypertension. *J Biomech* 36(5):671–680
- Gasser TC, Ogden RW, Holzapfel GA (2006) Hyperelastic modelling of arterial layers with distributed collagen fibre orientations. *J R Soc Interface* 3(6):15–35
- Hayashi K, Handa H, Nagasawa S, Okumura A, Moritake K (1980) Stiffness and elastic behavior of human intracranial and extracranial arteries. *J Biomech* 13(2):175–184
- Hoeks APG, Brands PJ, Willigers JM, Reneman RS (1999) Non-invasive measurement of mechanical properties of arteries in health and disease. *Proc Inst Mech Eng Part H* 213(3):195–202
- Holtackers RJ, Spronck B, Heusinkveld MHG, Crombag G, op 't Roodt J, Delhaas T, Kooi ME, Reesink KD, Hermeling E (2016) Head orientation should be considered in ultrasound studies on carotid artery distensibility. *J Hypertens* 34(8):1551–5
- Holzapfel GA, Ogden RW (2010) Constitutive modelling of arteries. *Proc R Soc A* 466(2118):1551–1597
- Holzapfel GA, Gasser TC, Ogden RW (2000) A new constitutive framework for arterial wall mechanics and a comparative study of material models. *J Elast* 61(1–3):1–48
- Holzapfel GA, Gasser TC, Stadler M (2002) A structural model for the viscoelastic behavior of arterial walls: continuum formulation and finite element analysis. *Eur J Mech A-Solid* 21(3):441–463
- Huberts W, Donders WP, Delhaas T, van de Vosse FN (2014) Applicability of the polynomial chaos expansion method for personalization of a cardiovascular pulse wave propagation model. *Int J Numer Methods Biomed Eng* 30(12):1679–1704
- Humphrey JD (2002) Cardiovascular solid mechanics: cells, tissues, and organs. Springer Science & Business Media, New York
- Humphrey JD, Harrison DG, Figueroa CA, Lacolley P, Laurent S (2016) Central artery stiffness in hypertension and aging a problem with cause and consequence. *Circ Res* 118(3):379–381
- Kass DA, Shapiro EP, Kawaguchi M, Capriotti AR, Scuteri A, Lakatta EG (2001) Improved arterial compliance by a novel advanced glycation end-product crosslink breaker. *Circulation* 104(13):1464–1470
- Kayed HR, Kirby N, Hawley A, Mudie ST, Haverkamp RG (2015) Collagen fibril strain, recruitment and orientation for pericardium under tension and the effect of cross links. *RSC Adv* 5(125):103703–103712
- Langewouters GJ, Zwart A, Busse R, Wesseling KH (1986) Pressure-diameter relationships of segments of human finger arteries. *Clin Phys Physiol Meas* 7(1):43
- McNulty M, Mahmud A, Feely J (2007) Advanced glycation end-products and arterial stiffness in hypertension. *Am J Hypertens* 20(3):242–247
- Meinders JM, Hoeks APG (2004) Simultaneous assessment of diameter and pressure waveforms in the carotid artery. *Ultrasound Med Biol* 30(2):147–154
- Moré JJ, Sorensen DC (1983) Computing a trust region step. *SIAM J Sci Stat Comput* 4(3):553–572
- National Research Council (2012) Assessing the reliability of complex models: mathematical and statistical foundations of verification, validation, and uncertainty quantification. National Academies Press, Washington
- O'Rourke MF, Hashimoto J (2007) Mechanical factors in arterial aging: a clinical perspective. *J Am Coll Cardiol* 50(1):1–13
- Patel DJ, Fry DL (1969) The elastic symmetry of arterial segments in dogs. *Circ Res* 24(1):1–8
- Quicken S, Donders WP, van Disseldorp EM, Gashi K, Mees BM, van de Vosse FN, Lopata RG, Delhaas T, Huberts W (2016) Application of an adaptive polynomial chaos expansion on computationally expensive three-dimensional cardiovascular models for uncertainty quantification and sensitivity analysis. *J Biomech Eng* 138(12):121010
- Sáez P, Peña E, Martínez M (2014) A structural approach including the behavior of collagen cross-links to model patient-specific human carotid arteries. *Ann Biomed Eng* 42(6):1158–1169
- Saltelli A, Ratto M, Andres T, Campolongo F, Cariboni J, Gatelli D, Saisana M, Tarantola S (2008) Global sensitivity analysis: the primer. John Wiley & Sons, Chichester
- Shadwick RE (1999) Mechanical design in arteries. *J Exp Biol* 202(23):3305–3313
- Silverman BW (1986) Density estimation for statistics and data analysis, 1st edn. Chapman & Hall, London
- Sobol IM (1967) On the distribution of points in a cube and the approximate evaluation of integrals. *Zhurnal Vychislitel'noi Matematiki i Matematicheskoi Fiziki* 7(4):784–802
- Sommer G, Holzapfel GA (2012) 3D constitutive modeling of the biaxial mechanical response of intact and layer-dissected human carotid arteries. *J Mech Behav Biomed* 5(1):116–128. doi:10.1016/j.jmbbm.2011.08.013
- Sommer G, Regitnig P, Köllringer L, Holzapfel GA (2010) Biaxial mechanical properties of intact and layer-dissected human carotid arteries at physiological and suprphysiological loadings. *Am J Physiol Cell Physiol* 298(3):H898
- Spronck B, Heusinkveld MHG, Donders WP, de Lepper AGW, Op't Roodt J, Kroon AA, Delhaas T, Reesink KD (2015a) A constitutive modeling interpretation of the relationship between carotid artery stiffness, blood pressure and age in hypertensive subjects. *Am J Physiol Heart Circ Physiol* 308:H568–H582
- Spronck B, Heusinkveld MHG, Vanmolkt FH, Op 't Roodt J, Hermeling E, Delhaas T, Kroon AA, Reesink KD (2015b) Pressure-dependence of arterial stiffness: potential clinical implications. *J Hypertens* 33(2):330–338
- Sudret B (2008) Global sensitivity analysis using polynomial chaos expansions. *Reliab Eng Syst Saf* 93(7):964–979
- Sudret B (2015) Polynomials chaos expansions and stochastic finite element methods. In: Phoon KK, Ching J (eds) Risk and Reliability in Geotechnical Engineering, Chap 6. Taylor and Francis, London, pp 265–300
- Takamizawa K, Hayashi K (1987) Strain energy density function and uniform strain hypothesis for arterial mechanics. *J Biomech* 20(1):7–17
- Townsend RR, Wilkinson IB, Schiffrin EL, Avolio AP, Chirinos JA, Cockcroft JR, Heffernan KS, Lakatta EG, McEniery CM, Mitchell GF, Najjar SS, Nichols WW, Urbina EM, Weber T (2015) Recommendations for improving and standardizing vascular research on arterial stiffness: a scientific statement from the American Heart Association. *Hypertension* 66:698–722
- van der Horst A, van den Broek CN, van de Vosse FN, Rutten MCM (2012) The fiber orientation in the coronary arterial wall at physiological loading evaluated with a two-fiber constitutive model. *Biomech Model Mechanobiol* 11(3–4):533–542
- Van Loon P (1976) Length-force and volume-pressure relationships of arteries. *Biorheology* 14(4):181–201
- Watton PN, Ventikos Y, Holzapfel GA (2009) Modelling the mechanical response of elastin for arterial tissue. *J Biomech* 42(9):1320–1325
- Weizsäcker HW, Lambert H, Pascale K (1983) Analysis of the passive mechanical properties of rat carotid arteries. *J Biomech* 16(9):703–715

Willekes C, Hoeks AP, Bots ML, Brands PJ, Willigers JM, Reneman RS (1999) Evaluation of off-line automated intima-media thickness detection of the common carotid artery based on m-line signal processing. *Ultrasound Med Biol* 25(1):57–64

Wolffenbuttel BH, Boulanger CM, Crijns FR, Huijberts MS, Poitevin P, Swennen GN, Vasan S, Egan JJ, Ulrich P, Cerami A, Levy BI (1998) Breakers of advanced glycation end products restore large artery properties in experimental diabetes. *Proc Natl Acad Sci U S A* 95(8):4630–4634